Chinese Chemical Letters 33 (2022) 3227–3230

Contents lists available at ScienceDirect

Chinese Chemical Letters

journal homepage: www.elsevier.com/locate/cclet

Flexible side arms of ditopic linker as effective tools to boost proton conductivity of Ni_8-pyrazolate metal-organic framework

Jieying Hu, Hu Zhang, Zihao Feng, Qian-Ru Luo, Can-Min Wu, Yuan-Hui Zhong, Jian-Rong Li, Lai-Hon Chung*, Wei-Ming Liao, Jun He*

School of Chemical Engineering and Light Industry, Guangdong University of Technology, Guangzhou 510006, China

ARTICLE INFO

Article history:
Received 18 September 2021
Revised 9 October 2021
Accepted 15 October 2021
Available online 22 October 2021

Keywords:
Proton conductivity
Metal-organic framework
Pyrazolate linkers
Nickel-oxide cluster
Imidazole encapsulation

ABSTRACT

Two primitive metal-organic frameworks (MOFs), Ni**L1** and Ni**L2**, based on Ni_8O_6-cluster and ditopic pyrazolate linkers, **L1** (with rigid alkyne arms) and **L2** (with flexible alkyne chains), were prepared. The proton conductivities of these MOFs in pristine form and imidazole-encapsulated forms, Im@Ni**L1** and Im@Ni**L2**, were measured and compared. Upon introduction of imidazole molecules, the proton conductivity could be increased by 3 to 5 orders of magnitude and reached as high as 1.72×10^{-2} S/cm (at 98% RH and 80 °C). Also, whether imidazole molecules were introduced or not, Ni_8O_6-based MOFs with **L2** in general gave better proton conductivity than those with **L1** signifying that flexible side arms indeed assist proton conduction probably *via* establishment of efficient proton-conducting channels along with formation of highly ordered domains of water/imidazole molecules within the network cavities. Beyond the active Ni_8O_6-cluster, tuning flexibility of linker pendants serves as an alternative approach to regulate/modulate the proton conductivity of MOFs.

Metal-organic frameworks (MOFs), constructed by metal ions and organic linkers, represent a fast-growing material because of their structural merits such as high crystallinity, tunable porosity, rich guest-host interaction and designable functionality [1–6]. Thanks to the unrelenting effort put on MOFs, it was found that hard-soft-acid-base (HSAB) theory applies well to be a guideline for MOF construction [7,8]. Specifically, hard donors match hard nodes well (*e.g.*, common UiO-network [9,10] from hard Zr(IV) ions and carboxylate-based linkers) while soft donors fit soft nodes (*e.g.*, renowned Zeolitic Imidazolate framework, ZIF [11,12], built from soft imidazolate linkers and Zn^{2+} nodes; M-pyrazolate MOFs [13–16] constructed from relatively soft metal ions like Cu^{+}, Ni^{2+}, Zn^{2+}, *etc.* and soft pyrazolate ligands). Even though MOFs of UiO-series are research hotspots because of their well-defined structure and ease of post-modification, this class of MOFs still suffers from instability sometimes for the vulnerability of Zr-O cluster towards the complex surrounding environment [8,17]. On the other hand, MOFs established from soft precursors feature structural parameters (*e.g.*, porosity, type of cluster nodes, acidity of the nodes) different from those UiO-frameworks and sometimes express higher stability than UiO-analogues in a wide range of conditions [18,19]. These classes of MOFs have been being extensively investigated in the field of porous coordination polymers and their applications.

Among various applications, developing MOFs as proton conductors recently become a research hotspot because of the following reasons: (1) High porosity of MOFs allows introduction of proton-conducting guest ions/molecules to enhance proton conductivity; (2) Rich tunability of linkers confers framework potentials for modulation of stability and functionality. To utilize the unique porosity of MOFs, loading of guest molecules/ions represents one of the most effective strategies to enhance the proton conductivity of the framework materials [20–29]. Recently, it has been demonstrated that introduction of imidazole-type molecules into framework successfully improves the proton conductivity of the MOFs by as high as 10^{-1}∼10^{-3} S/cm in the range of 30∼100 °C and relative humidity (RH) of 98%∼100% [30–35]. Imidazole molecules, encapsulated in voids, can serve as proton carriers themselves or pack orderly to form proton-conducting channels just like the most primitive proton conductor–water molecule does. Hence, imidazole and water molecules carry out proton conduction through the same mechanistic options [36]. Interestingly, there arises a new improvement approach in which hydrophobicity of framework assists proton conduction by minimizing host-guest interaction and promotes regular packing of guest molecules into ordered proton-conducting channels for better proton conductivity [37,38]. The combination of guest molecules and hydrophobicity of

* Corresponding authors.
E-mail addresses: laihonchung@gdut.edu.cn (L.-H. Chung), junhe@gdut.edu.cn (J. He).

https://doi.org/10.1016/j.cclet.2021.10.042
1001-8417/

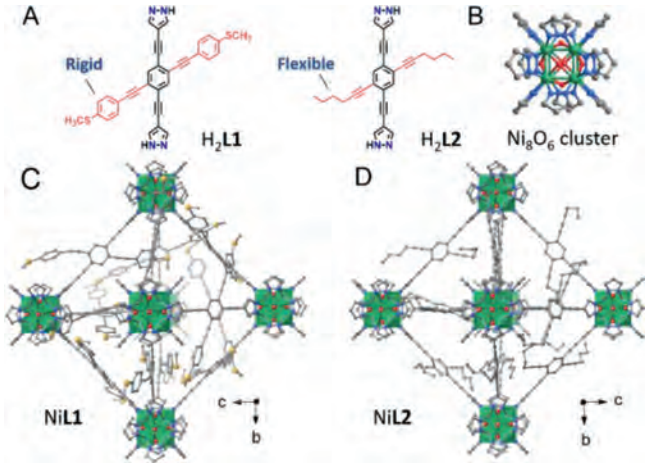

Fig. 1. (A) Structures of ditopic linkers, H_2**L1** and H_2**L2**, featuring rigid aromatic side arms and flexible alkyl chains, respectively. (B) A $Ni_8(OH)_4(H_2O)_2$ (abbreviated as Ni_8O_6) cluster with 12 associated pyrazolate units. (C, D) view of an octahedral unit in an idealized model (*i.e.*, assuming full linker occupancy) of the **fcu** net of Ni**L1** and Ni**L2** along *a* axis. H atoms were omitted for clarity. Red spheres, O; gray, C; blue, N; yellow, S; green, Ni/Ni-based polyhedral.

framework may turn to be a novel strategy for rational design of proton conducting MOFs.

When it comes to M-pyrazolate MOFs, those based on face-centered cubic (fcc) $[Ni_8(OH)_4(H_2O)_2]^{12+}$ (Ni_8O_6) cluster and ditopic pyrazolate ligands represent a class of chemically stable materials [8,18,19]. Gratifyingly, the Ni_8O_6 cluster in this class of stable MOFs has been found active in both proton and hydroxide conductivity [39,40]. However, these works only focused on the function of Ni_8O_6 cluster and omitted the possible contribution from the design of the ditopic pyrazolate linkers. Our group previously reported a Ni_8O_6-based MOF, Ni**L1** (Fig. 1A for the ligand H_2**L1**; Fig. 1C for the structure of Ni**L1**), established from ditopic pyrazolate linkers with specially designed side arms. Considering **L1**, pyrazolate on both terminals of course serve to form coordination bonds with the clusters while the alkyne side chains were set to control the porosity of the network. As our plan goes, Ni**L1** exhibited excellent tolerance in a range of conditions (*e.g.*, solution of extreme pH values and exposure to high temperature) [41]. Combining our previous experimental findings and going beyond Ni_8O_6-cluster, we aim to develop Ni_8O_6-based MOF as active proton conductor with rational design of the alkyne pendants on ditopic pyrazolyl linker.

Herein, we propose to use **L2** (Fig. 1A), structurally analogous to **L1**, as linker to construct Ni_8O_6-based MOF, Ni**L2**, and compare with Ni**L1** for proton conductivity of their primitive forms and imidazole-encapsulated forms, Im@Ni**L1** and Im@Ni**L2**. Looking at **L2**, the main skeleton is identical to **L1,** but the pendants are set to bear flexible alkyl chains instead of rigid aromatic side arms (Fig. 1A). The flexible alkyl chains within Ni**L2** network are expected to act as dynamic regulators in the voids and thus facilitate arrangement of imidazole and water molecules into well-organized channels beneficial to proton conduction. This effect is thought to be absent in the network of Ni**L1** because rigid pendants are fixed in space and fail to complement upcoming imidazole molecules for building efficient proton-conducting channels. This work aims to verify how flexible hydrophobic pendants help proton conduction of MOF when compared with rigid hydrophobic pendants.

Following a similar synthetic strategy of Ni**L1** [41], the dark yellow crystalline powder of Ni**L2** was obtained *via* solvothermal reaction between Boc_2**L2** molecules and $Ni(OAc)_2{\cdot}4H_2O$ using *N*,*N*-dimethylacetamide (DMA) and H_2O as solvent. Powder X-ray diffraction (PXRD) reveals that Ni**L2** has a cubic lattice

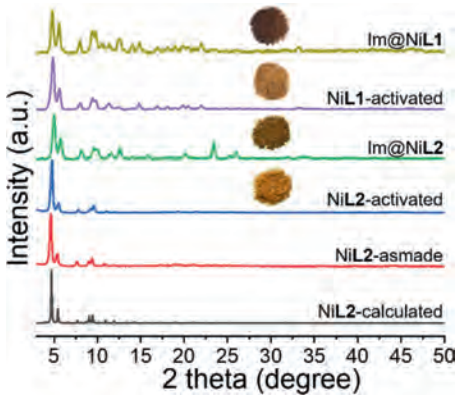

Fig. 2. PXRD patterns (Cu Kα, $\lambda = 1.5418$ Å) for the crystal structure model of Ni**L2**, as-made sample of Ni**L2**, activated sample of Ni**L2**, imidazole-loaded sample of Ni**L2** (Im@Ni**L2**), activated sample of Ni**L1** and imidazole-loaded sample of Ni**L1**, (Im@Ni**L1**). Inset: photographs of corresponding samples.

($a = b = c = 32.3556$ Å, Fig. 2, details of refinement are included in Supporting information). With reference to previously reported Ni_8O_6-cluster-based MOFs [18,19,40,42,43], a crystal structure of Ni**L2** is modelled based on $[Ni_8(OH)_4(H_2O)_2]$ node (Fig. 1B) and the final network (Fig. 1D) is found isoreticular to reported Ni(II)-MOFs having the **fcu** topology with fcc array of the Ni_8O_6 clusters [44–46].

Elemental analysis of an activated sample of Ni**L2** suggested the chemical formula to be $Ni_8(OH)_4(H_2O)_2$(**L2**)$_{3.45}(CH_3COO)_{5.1}(H_2O)_{16}$. The high H_2O content may originate from atmospheric moisture and the CH_3COO^- probably come from decomposition of DMA at high temperature. The origin of CH_3COO^- inside the framework is verified by NMR experiments (Fig. S9 in Supporting information) and these suggest that CH_3COO^- are coordinating ligands rather than free ions present in channels. In a perfect **fcu** net, Ni_8O_6 cluster in combination with **L2** normally gives a formula of $Ni_8(OH)_4(H_2O)_2$(**L2**)$_6$ in which the Ni_8O_6 cluster is connected to 12 pyrazolate units (provided by 6 ditopic **L2**). However, the current Ni**L2** only bears 7 pyrazolate units from 3.5 **L2** and the remaining sites are occupied by 5 CH_3COO^- ligands as reflected by the determined formula. Mixed carboxyl/pyrazolate ligands on Ni_8O_6 cluster have been reported [45] and the linker deficiency in Ni**L2** most likely results from steric hindrance exerted by the long alkyne side arms which limit the number of linkers approaching the Ni_8O_6-cluster. It is noted that lower linker deficiency in Ni**L2** (42.5%) when compared with Ni**L1** (50%) is likely attributed to less steric bulkiness in **L2** than **L1**. Noteworthy, both Ni**L1** and Ni**L2** are stable in a wide range of condition as reflected by their PXRD patterns after being immersed in boiling water, extremely acidic/alkaline solution, and even thermal treatment at 320 °C for 2 h (no significant peaks broadening of PXRD patterns, Fig. S10 in Supporting information). The extraordinary stability of Ni**L1** and Ni**L2** highlight their potentials as carriers to house imidazole.

Imidazole molecules were introduced into Ni**L1** and Ni**L2** through thermally assisted vaporization of imidazole molecules under reduced pressure to give Im@Ni**L1** and Im@Ni**L2** respectively. The similar PXRD patterns of Ni**L1**/Ni**L2** and Im@Ni**L1**/Im@Ni**L2** confirm framework integrity of Ni**L1**/Ni**L2** after introduction of imidazole molecules (Fig. 2). From Ni**L1**/Ni**L2** to Im@Ni**L1**/Im@Ni**L2**, the rise of IR stretching signals at 1068/1057, 1324/1327 and 3133/3140 cm^{-1} is indicative of successful introduction of imidazole molecules into Ni**L1**/Ni**L2** because these three peaks correspond to C–N, C–N–C and N–H stretching of imidazole (Figs. S12 and S14 in Supporting information) [32,35]. Importantly, N_2 adsorption-desorption isotherms at 77 K reveal that both Ni**L2** and Im@Ni**L2** display type-I sorption isotherm. The Brunauer-Emmett-

Teller (BET) surface area and the pore volume of Ni**L2** are 1364.6 m^2/g and 0.771 cm^3/g respectively while those of Im@Ni**L2** are 49.54 m^2/g and 0.217 cm^3/g, respectively (Figs. S16-S19 in Supporting information). The decrease in surface area and pore volume from Ni**L2** to Im@Ni**L2** supports the encapsulation of imidazole molecules in Ni**L2**. Besides, scanning electron microscope (SEM) images illustrate that the morphology of Im@Ni**L2** is like that of pristine Ni**L2** without obvious change of the surface (Fig. S20 in Supporting information), suggesting that there exist no aggregates of imidazole molecules on the surface. The above experimental evidence consolidates the successful encapsulation of imidazole guests in Ni**L1**/Ni**L2**; yet the possibility of trace imidazole molecules left on the surface of framework should not be excluded.

Even though it has been proved that the imidazole molecules are located inside the voids of network, it is necessary to resolve the quantity of imidazole molecules introduced. Thermogravimetric analysis (TGA) of Im@Ni**L1**/Im@Ni**L2** (Figs. S21 and S22 in Supporting information) showed that there are *ca.* 16.4 imidazole molecules per unit of Ni**L1** and *ca.* 16.8 imidazole molecules per unit of Ni**L2** respectively. Both Ni**L1** and Ni**L2** could host similar quantities of imidazole molecules demonstrating comparable guest molecules housing capacity. Water affinity of all four samples were compared by their water contact angles and it was found that Im@Ni**L1**/Im@Ni**L2** have smaller contact angles than Ni**L1**/Ni**L2** (Fig. S23 in Supporting information) reflecting higher hydrophilicity of Im@Ni**L1**/Im@Ni**L2** than Ni**L1**/Ni**L2**. Given that the imidazole molecules have been introduced into the cavities inside Ni**L1**/Ni**L2** successfully, Im@Ni**L1**/Im@Ni**L2** serves as a good candidate for proton conductivity study.

To investigate how encapsulation of imidazole molecules enhance the proton conductivities of Ni**L1**/Ni**L2**, AC impedance spectroscopy has been conducted on freshly prepared pellets of Ni**L1**/Ni**L2** and Im@Ni**L1**/Im@Ni**L2** under different RH (in the range of 30% to 90%) at 90 °C and at different temperatures (in the range of 30 °C to 80 °C) under 98% RH. Nyquist plots of all four samples under different RH (from 30% to 90%) at 90 °C show an increase in proton conductivity (σ) (Fig. S36 in Supporting information). From RH of 30% to 90% at 90 °C, σ of Ni**L1** and Ni**L2** increase by 2 to 3 orders of magnitude until 10^{-8} S/cm while those of Im@Ni**L1** and Im@Ni**L2** increase by 3 to 5 orders of magnitude until 10^{-5} S/cm and 10^{-3} S/cm, respectively (under 90% RH at 90 °C, 1.17×10^{-8} S/cm for Ni**L1**, 8.82×10^{-8} S/cm for Ni**L2**, 7.42×10^{-5} S/cm for Im@Ni**L1** and 1.00×10^{-3} S/cm for Im@Ni**L2**, Table S1 in Supporting information). Enhancement of σ along with increasing RH is reasonable as water molecules are packed more closely under higher RH and this provides more channels for proton conduction. Noteworthy, when the RH is fixed at 98%, the Nyquist plots of all samples at different temperature (from 30 °C to 80 °C) show a similar trend in σ (Fig. S37 in Supporting information). From 30 °C to 80 °C under RH of 98%, σ of Ni**L1** and Ni**L2** also increase by 2 to 3 orders of magnitude but reach maximal σ of 10^{-5} S/cm while those of Im@Ni**L1** and Im@Ni**L2** (Fig. 3) increase by 1 to 3 orders of magnitude until 10^{-3} S/cm and 10^{-2} S/cm (under 98% RH at 80 °C, 2.46×10^{-8} S/cm for Ni**L1**, 1.41×10^{-5} S/cm for Ni**L2**, 1.86×10^{-3} S/cm for Im@Ni**L1** and 1.72×10^{-2} S/cm for Im@Ni**L2**, Table S2 in Supporting information). At fixed 98% RH, water molecules are sufficiently available for proton conduction and elevating temperature indeed facilitate the proton conduction because protons with higher kinetic energy inside the channels are more active. The σ of the imidazole-encapsulated MOFs reported in this work lie in the sample range as expressed by other imidazole-housing MOFs (Table S3 in Supporting information). To our knowledge, our results represent the best example to date considering the boost of σ by introduction of imidazole molecules into Ni-based MOF [47]. Also, it is noted that generally higher σ of Im@Ni**L1**/Im@Ni**L2** than Ni**L1**/Ni**L2** regardless of RH and temperature highlight the supremacy of imidazole molecules in framework as promoter for proton conductivity.

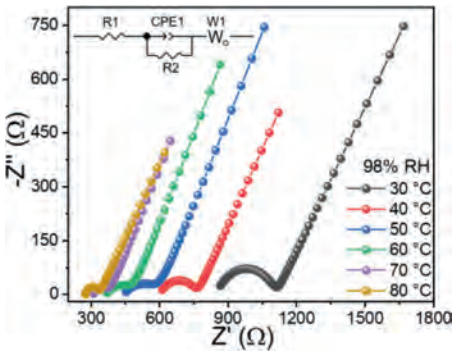

Fig. 3. Nyquist plots of Im@Ni**L2** at 30~80 °C under 98% RH.

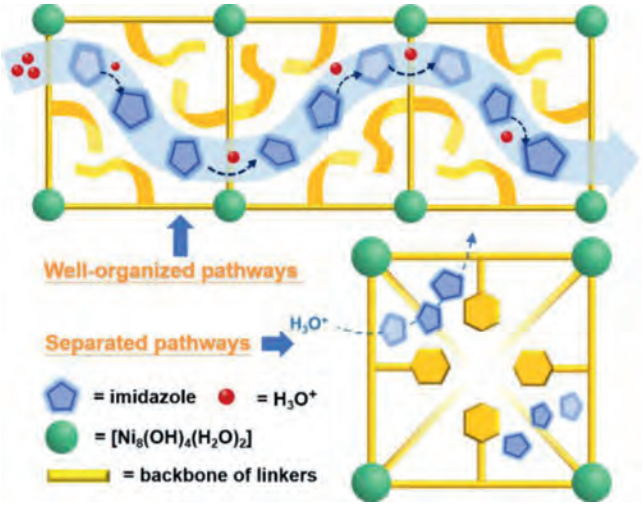

Fig. 4. A schematic representation of arrangement of imidazole guests during loading and possible proton conduction mode in the pores of Ni**L1** (bottom) and Ni**L2** (top).

To rationalize the proton conduction mechanisms in these materials, the Arrhenius plots in a linear relationship [$\ln(\sigma T)$ *vs.* $1000T^{-1}$] are plotted (Figs. S26, S29, S32 and S34 in Supporting information). Noteworthy, the activation energy (E_a) of Ni**L1**, Ni**L2**, Im@Ni**L1** and Im@Ni**L2** under 98% RH are found to be 0.82, 1.20, 1.29 and 0.30 eV respectively. It is well-established that E_a of 0.1~0.4 eV corresponds to Grotthuss mechanism where protons are conducted along water channels in a way of proton-jump/hopping whereas E_a of >0.4 eV follows the Vehicle mechanism in which protic molecules serve as proton carriers and diffuse for transporting protons [48,49]. Ni**L1**, Ni**L2** and Im@Ni**L1** follow Vehicle mechanism while Im@Ni**L2** adopts Grotthuss mechanism for proton conduction. Presumably, flexible alkyl chains in **L2** assisted organization of imidazole along with water molecules and gave rise to well-organized imidazole-water channels for efficient proton hopping while rigid pendants in **L1** failed to coordinate the ordered arrangement of water and imidazole molecules for efficient proton jump (Fig. 4). It is worth-mentioning that **L2** itself without introduction of imidazole molecules bearing hydrophobic pendants minimally interact with water molecules effectively promoting formation of ordered domains of water molecules as proton-hopping channels. These are possible rationales to explain the proton conducting mechanisms adopted by all four samples reported in this work. These results undoubtedly stand out the function of flexible pendants on linker for coordinating guest introduction and hence facilitating proton conduction within network.

In summary, Ni_8O_6-pyrazolate MOFs, Ni**L1** and Ni**L2**, were prepared and investigated the proton conductivity of their pristine forms and imidazole-encapsulated forms, Im@Ni**L1** and Im@Ni**L2**. It was found that introduction of imidazole molecules into network of Ni**L1** and Ni**L2** effectively boost the proton conductivity for mostly 3 to 5 orders of magnitude to at most 1.72×10^{-2} S/cm (at 98% RH and 80 °C). Reflected by the activation energies, Ni**L1**, Ni**L2** and Im@Ni**L1** were rationalized to opt for Vehicle mechanism while Im@Ni**L2** probably adopted Grotthuss mechanism as major ways for proton conduction. The difference in the proton-conducting mechanism probably arises from coordinating packing of imidazole and water molecules by flexible alkyl side arms on **L2** during introduction of guest imidazole. This work highlights the success of our strategy on modulating proton conductivity of network through side arms engineering and represents a vivid example of adjusting proton conductivity of MOFs by regulating the microenvironment of voids in MOF.

Declaration of competing interest

The authors declare that they have no known competing financial interests or personal relationships that could have appeared to influence the work reported in this paper.

Acknowledgments

This work was supported by the National Natural Science Foundation of China (No. 21871061), the Foundation of Basic and Applied Basic Research of Guangdong Province (No. 2021A1515010274), the Local Innovative and Research Teams Project of Guangdong Pearl River Talents Program (No. 2017BT01Z032), the Science and Technology Planning Project of Guangdong Province (No. 2021A0505030066), and the Science and Technology Program of Guangzhou (No. 201807010026).

Supplementary materials

Supplementary material associated with this article can be found, in the online version, at doi:10.1016/j.cclet.2021.10.042.

References

[1] O.M. Yaghi, H. Li, J. Am. Chem. Soc. 117 (1995) 10401–10402.
[2] P.I. Scheurle, A. Mähringer, A. Biewald, et al., Chem. Mater. 33 (2021) 5896–5904.
[3] W. Zhao, J. Peng, W. Wang, et al., Coord. Chem. Rev. 377 (2018) 44–63.
[4] J.D. Xiao, H.L. Jiang, Acc. Chem. Res. 52 (2019) 356–366.
[5] R. Newar, N. Akhtar, N. Antil, et al., Angew. Chem. Int. Ed. 60 (2021) 10964–10970.
[6] P.Q. Liao, J.Q. Shen, J.P. Zhang, Coord. Chem. Rev. 373 (2018) 22–48.
[7] P.K. Chattaraj, H. Lee, R.G. Parr, J. Am. Chem. Soc. 113 (1991) 1855–1856.
[8] S. Yuan, L. Feng, K. Wang, et al., Adv. Mater. 30 (2018) 1704303.
[9] J.H. Cavka, S.R. Jakobsen, U. Olsbye, et al., J. Am. Chem. Soc. 130 (2008) 13850–13851.
[10] V. Guillerm, S. Gross, C. Serre, et al., Chem. Commun. 46 (2010) 767–769.
[11] K.S. Park, Z. Ni, A.P. Côté, et al., Proc. Natl. Acad. Sci. 103 (2006) 10186–10191.
[12] R. Banerjee, A. Phan, B. Wang, et al., Science 319 (2008) 939–943.
[13] T. He, Z. Huang, S. Yuan, et al., J. Am. Chem. Soc. 142 (2020) 13491–13499.
[14] S. Mukherjee, Y. He, D. Franz, et al., Chem. Eur. J. 26 (2020) 4923–4929.
[15] J.P. Zhang, S. Kitagawa, J. Am. Chem. Soc. 130 (2008) 907–917.
[16] J.P. Zhang, S. Horike, S. Kitagawa, Angew. Chem. Int. Ed. 46 (2007) 889–892.
[17] T. He, X.J. Kong, J.R. Li, Acc. Chem. Res. 54 (2021) 3083–3094.
[18] X.L. Lv, K. Wang, B. Wang, et al., J. Am. Chem. Soc. 139 (2017) 211–217.
[19] K. Wang, X.L. Lv, D. Feng, et al., J. Am. Chem. Soc. 138 (2016) 914–919.
[20] A. Shigematsu, T. Yamada, H. Kitagawa, J. Am. Chem. Soc. 133 (2011) 2034–2036.
[21] J.M. Taylor, K.W. Dawson, G.K.H. Shimizu, J. Am. Chem. Soc. 135 (2013) 1193–1196.
[22] M. Bazaga-García, R.M.P. Colodrero, M. Papadaki, et al., J. Am. Chem. Soc. 136 (2014) 5731–5739.
[23] W.J. Phang, H. Jo, W.R. Lee, et al., Angew. Chem. Int. Ed. 54 (2015) 5142–5146.
[24] H.Q. Zhou, Y. He, J.Y. Hu, et al., Chem. Commun. 57 (2021) 187–190.
[25] B. Joarder, J.-.B. Lin, Z. Romero, et al., J. Am. Chem. Soc. 139 (2017) 7176–7179.
[26] F. Yang, G. Xu, Y. Dou, et al., Nat. Energy 2 (2017) 877–883.
[27] T. Yamada, K. Otsubo, R. Makiura, et al., Chem. Soc. Rev. 42 (2013) 6655–6669.
[28] W.H. Li, W.H. Deng, G.E. Wang, et al., EnergyChem 2 (2020) 100029.
[29] B.B. Hao, X.X. Wang, C.X. Zhang, et al., Cryst. Growth Des. 21 (2021) 3908–3915.
[30] F.M. Zhang, L.Z. Dong, J.S. Qin, et al., J. Am. Chem. Soc. 139 (2017) 6183–6189.
[31] Y. Ye, W. Guo, L. Wang, et al., J. Am. Chem. Soc. 139 (2017) 15604–15607.
[32] H.B. Luo, Q. Ren, P. Wang, et al., ACS Appl. Mater. Interfaces 11 (2019) 9164–9171.
[33] J. Cao, W. Ma, K. Lyu, et al., Chem. Sci. 11 (2020) 3978–3985.
[34] Z. Zhang, J. Ren, J. Xu, et al., J. Membr. Sci. 607 (2020) 118194.
[35] T.H.N. Lo, M.V. Nguyen, T.N. Tu, Inorg. Chem. Front. 4 (2017) 1509–1516.
[36] V.G. Ponomareva, K.A. Kovalenko, A.P. Chupakhin, et al., J. Am. Chem. Soc. 134 (2012) 15640–15643.
[37] T. Homburg, C. Hartwig, H. Reinsch, et al., Dalton Trans. 45 (2016) 15041–15047.
[38] K.-.I. Otake, H. Kitagawa, Small 17 (2021) 2006189.
[39] C. Montoro, P. Ocón, F.L. Zamora, et al., Chem. Eur. J. 22 (2016) 1646–1651.
[40] T. He, Y.Z. Zhang, H. Wu, et al., ChemPhysChem 18 (2017) 3245–3252.
[41] J. Hu, X. Deng, H. Zhang, et al., Inorg. Chem. 60 (2021) 161–166.
[42] N. Huang, K. Wang, H. Drake, et al., J. Am. Chem. Soc. 140 (2018) 6383–6390.
[43] Y.Z. Zhang, T. He, X.J. Kong, et al., ACS Mater. Lett. 1 (2019) 20–24.
[44] N. Masciocchi, S. Galli, V. Colombo, et al., J. Am. Chem. Soc. 132 (2010) 7902–7904.
[45] N.M. Padial, E. Quartapelle Procopio, C. Montoro, et al., Angew. Chem. Int. Ed. 52 (2013) 8290–8294.
[46] E. López-Maya, C. Montoro, V. Colombo, et al., Adv. Funct. Mater. 24 (2014) 6130–6135.
[47] Z. Bai, S. Liu, P. Chen, et al., Nanotechnology 31 (2020) 125702.
[48] K.D. Kreuer, A. Rabenau1W. Weppner, Angew. Chem. Int. Ed. 21 (1982) 208–209.
[49] D.K. Paul, A. Fraser1K. Karan, Electrochem. Commun. 13 (2011) 774–777.